Appl. Phys. B 66, 701–710 (1998)

Applied Physics B
Lasers
and Optics

Continuous-wave, intracavity optical parametric oscillators: an analysis of power characteristics

G.A. Turnbull, M.H. Dunn, M. Ebrahimzadeh

The J.F. Allen Physics Research Laboratories, School of Physics & Astronomy, University of St Andrews, Fife, KY16 9SS, UK
(Fax: +44-1334/463-104, E-mail: gat@st-and.ac.uk)

Received: 29 December 1997/Revised version: 6 February 1998

Abstract. We describe the steady-state and transient power characteristics of continuous-wave intracavity singly resonant parametric oscillators (ICSROs). The operation characteristics of recently demonstrated ICSROs are reviewed. We derive a rate-equation model for the ICSRO which features a multi-frequency laser field. The steady-state behaviour of the device is detailed and methods to optimise the signal and idler outputs are presented. A Liapunov analysis tests the high-power stability of the system. We find that ICSROs do not suffer from the problems of instability which are characteristic of other intracavity frequency-mixing schemes and, as such, represent practical continuous-wave sources capable of high output powers and conversion efficiencies. Finally, we quantify the level of practical stability through an analysis of the novel transient behaviour of the ICSRO. We find that, to optimise the power stability, the signal cavity lifetime should be made as large as possible.

PACS: 42.65.Yj; 42.60.-v; 42.60.Lh

Intracavity frequency-conversion has long been established as an efficient method for generating continuous-wave (cw) visible light. Recent demonstrations of intracavity optical parametric oscillators (ICOPOs) have extended this approach to produce cw light tunable through the infrared [1–7]. The intense optical field within the pump laser cavity permits the use of a singly resonant OPO (SRO) geometry, avoiding the usual resonance constraints of cw doubly resonant OPOs (DROs). The resulting systems have exhibited Watt-level, amplitude-stable output powers with high quantum efficiencies, while single-frequency outputs have been demonstrated within crude multi-frequency pump-lasers.

In this paper we describe the steady-state and transient power characteristics of the cw ICSRO, principally through the development of a theoretical model. In Sect. 1 we review the experimental and theoretical progress in ICOPOs to the present date. In particular, attention is paid to the operation characteristics of the recently demonstrated ICSROs. All but one of these devices [2] have been based upon standing-wave laser resonators which feature multi-frequency laser fields. In Sect. 2 we develop a rate-equation model for the ICSRO which features such a multi-mode laser. Our model is in the spirit of those of [8–11] where the interacting waves adopt a particular fixed phase-relationship and dynamics occur on a scale of the cavity lifetimes. In Sects. 3 and 4 we analyse the steady-state behaviour of the ICSRO, and show how it may be optimised to give very high output-power efficiencies.

It is well known, however, that at high powers intracavity up-conversion can suffer from dynamic instabilities [9, 10]. These cause the erratic amplitude fluctuations of the "green problem", and present design constraints to the power-scaling of such systems. It was shown previously [8] that intracavity DROs (ICDROs) exhibit similar instabilities at moderate pumping levels. While the demonstrations of ICSROs at a pumping level of a few times the OPO threshold have shown that stable operation is possible, it can not rule out instabilities at higher pump levels. In Sect. 5 we address this issue of high-power stability through an analysis similar to [8, 10]. We find that ICSROs do not suffer from the same problems of instability and, as such, represent practical cw sources capable of high output powers and conversion efficiencies. Section 6 aims to quantify the level of practical stability through an analysis of the novel transient behaviour of the ICSRO.

1 Summary of cw ICOPOs

The operation a cw OPO internal to a laser cavity was first considered in a theoretical paper on the ICDRO by Oshman and Harris [8] in 1968. Their analysis found that, in addition to the resonance constraints normally associated with external-cavity DROs, such devices exhibit instabilities at moderate pumping levels. They showed that the ICDRO could operate in three different regimes when pumped above OPO threshold. First, there are two stable steady-state modes of operation: the efficient and inefficient regimes; second, there is an unstable, repetitively self-pulsing mode. The steady-state regimes are distinguished by the relative phase $\Delta\phi = \phi_p - \phi_s - \phi_i$ between the driving pump laser frequency ω_p, and generated signal, and idler frequencies, ω_s, ω_i, respectively. For the efficient regime, $\Delta\phi$ is fixed at $\pi/2$ which

optimises the nonlinear coupling. The inefficient regime is characterised by $\Delta\phi \neq \pi/2$; the parametric interaction drives the phases rather than the amplitudes and departs further from maximum conversion with increasing pump power. The pulsing mode produces a train of sub-microsecond pulses when the ICDRO is pumped ≈ 3 times above OPO threshold, limiting the potential for high-power cw operation of such a device. The relative magnitudes of cavity losses and laser and parametric gains determine in which regime the ICDRO will operate.

Soon after that paper, several demonstrations of ICDROs were reported in both cw and Q-switched lasers [12–15]. At this time Falk et al. [15] demonstrated a pulsed ICSRO based on a Q-switched laser. Subsequently, a theoretical analysis [16] of phase fluctuations in the ICDRO was published.

More recently, work has concentrated on ICSROs. These are free of the resonance constraints of DROs and so have the potential to form more practical devices, provided that the higher power thresholds may be surpassed. The next reported work on ICOPOs was a theoretical treatment in 1984 [17] of conversion efficiency and optimum focusing in cw ICSROs. This was followed by the first demonstration of a fs OPO [18] and further work on Q-switched ICSROs [11, 19]. This paper extends the work in [11, 17] to accommodate multi-frequency pump fields and addresses, for the first time, cw ICSRO power stability and relaxation oscillations.

The first cw ICSRO was reported by Colville et al. in 1996 [1]. This device was based on a KTP crystal pumped at the intracavity focus of a Ti:sapphire laser. When pumped above OPO threshold, the device exhibited the characteristic clamping of the laser field at the threshold level [20]. An output power of 400 mW was achieved with an amplitude stability of ±8% over a 50-s time-scale. The multi-mode laser-pump field was shown to couple through a single-mode signal field to generate an idler of the same bandwidth as the pump.

The power and tuning characteristics of this, and subsequently reported devices, are shown in Table 1. These feature ICSROs based on both birefringently phase-matched [1–3, 5] and the new quasi-phase-matched [4, 6, 7] materials. The former have relied on the tunability of the pump source for wavelength tuning. The latter have allowed tuning with fixed-wavelength lasers [4] and multi-parameter pump and grating tuning in [6].

Total down-converted powers at the Watt level have been demonstrated with very high conversion efficiencies [3, 4]. The ICSRO is typically less demanding of the pump laser power or spectral characteristics than are external cavity PPLN SROs [21, 22], since the latter require either multi-Watt or single-frequency pump sources to exceed threshold. This potential to operate SROs with relatively crude, moderate-power lasers makes the intracavity approach an attractive alternative to the external cavity SRO.

2 Derivation of multi-mode ICSRO model

We extend the derivation of the dynamical equations in [11] to accommodate a multi-frequency pump laser field (for example caused by spatial-hole-burning in a homogeneously broadened gain medium). The laser bandwidth is assumed to be well within the spectral acceptance bandwidth of the parametric interaction, allowing all laser modes to couple through a single-frequency, resonant signal [1, 3]. Figure 1 shows the schematic arrangement of the ICSRO. The device comprises a pump laser of length L_p which is in turn pumped by an external laser source, and an OPO cavity of length L_s in which the signal field is resonant and the idler field exits after a single pass. The high-finesse laser and OPO cavities share a common end mirror and are separated by a beamsplitter. A nonlinear crystal of length l is situated in the common arm

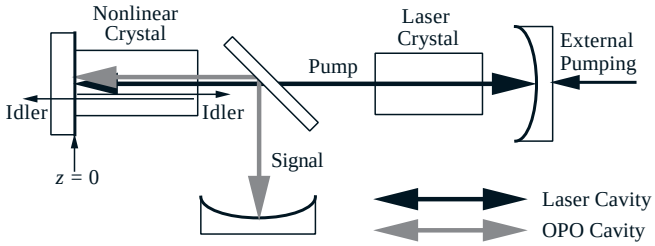

Fig. 1. Schematic arrangement of the ICSRO

Table 1. Powers and tuning characteristics of cw ICSROs

External pump	Laser	Nonlinear crystal	Wavelength: signal range Idler range	Output powers	Conversion efficiency	Ref.
Ar^+-Ion	Ti:sapphire	KTP	1.09–1.21 μm	270 mW	70%	[1, 3]
14 W		20 mm	2.53–2.87 μm	350 mW		
Ar^+-Ion	Rh6G	KTP	1.03–1.04 μm	28 mW	—	[2]
—		12 mm	1.25–1.37 μm	—		
Ar^+-Ion	Ti:sapphire	KTA	1.10–1.25 μm	500 mW	> 85%	[3]
14 W		12 mm	2.32–3.00 μm	800 mW		
Diode	Nd:YVO_4	PPLN	1.56–1.60 μm	—	—	[4]
30 A		25 mm	3.18–3.33 μm	850 mW		
Diode	Nd:YLF	KTA	1.50 μm	150 mW	70%	[5]
7 W		15 mm	3.47 μm	220 mW		
Ar^+-Ion	Ti:sapphire	PPLN	1.07–1.28 μm	50 mW	75%	[6]
6 W		19 mm	2.30–3.33 μm	240 mW		
DPSSL	Ti:sapphire	PPLN	1.07–1.28 μm	—	50%	[6]
5.1 W		19 mm	2.30–3.33 μm	100 mW		
Ar^+-Ion	Ti:sapphire	PPRTA	1.13–1.27 μm	—	43%	[7]
8 W		4.5 mm	2.53–3.26 μm	200 mW		

and, to simplify the algebra, the cavities and crystal share a common end at $z = 0$.

We define the laser and signal fields as

$$E_{\rm p}(z,r,t) = \sum_j 2E_{{\rm p}j}(t)\exp(-r^2/w_{\rm p}^2)\sin(k_{{\rm p}j}z) \times \cos(\omega_{{\rm p}j}t+\phi_{{\rm p}j})\,, \quad (1)$$

$$E_{\rm s}(z,r,t) = 2E_{\rm s}(t)\exp(-r^2/w_{\rm s}^2)\sin(k_{\rm s}z)\cos(\omega_{\rm s}t+\phi_{\rm s})\,. \quad (2)$$

Here, the subscript j denotes the jth laser mode, $k_{{\rm p},{\rm s}j} = n_{\rm p,s}\omega_{{\rm p}j,{\rm s}}/c$, and $n_{\rm p,s}$ is an effective refractive index, averaged over the cavity to avoid boundary problems. $w_{\rm p}$ and $w_{\rm s}$ are the sizes, respectively, of the laser and signal transverse waist radii in the nonlinear crystal.

We choose to set the signal to be a single-frequency field because we have found in practice [1, 3] this to be the most common mode of operation when the laser bandwidth is much less than the spectral acceptance bandwidth of the parametric interaction. Additionally, we have shown that the use of étalons in the OPO cavity can ensure stable single-frequency signal operation [3].

The use of such a single-mode signal implies that the OPO generates a single idler frequency $\omega_{{\rm i}j}$ for each $\omega_{{\rm p}j}$. We note that other nonlinear processes do take place in the ICSRO, where the jth laser mode mixes with the kth idler $j \neq k$. However these normally have a negligible effect since they do not feed energy into a cavity axial mode. They are only significant in the special case where the laser and OPO cavity lengths are in a low integral ratio. For in this arrangement $\omega_{{\rm p}j} - \omega_{{\rm i}k}$ matches another resonant frequency of the OPO cavity, which we find experimentally can allow sustained multi-mode signal operation. In general, however, the pump laser and OPO cavity lengths are not in such an integral ratio, $\omega_{{\rm p}j} - \omega_{{\rm i}k}$ does not match a resonance, and additional signal frequencies tend to be suppressed by the signal cavity.

The three interacting fields mix in the nonlinear medium to generate a polarisation

$$\mathcal{P}_{\rm i,s,p} = 2\varepsilon(2d_{\rm eff})E_{\rm p,i,s}(z,r,t)E_{\rm s,p,i}(z,r,t)\,. \quad (3)$$

Only the travelling-wave components of the resonant fields which propagate in the same direction interact, and we retain only the terms which satisfy $\omega_{{\rm p}j} = \omega_{\rm s} + \omega_{{\rm i}j}$. $\mathcal{P}_{\rm i}(z,r,t) = \mathcal{P}_{\rm i}^{+}(z,r,t) + \mathcal{P}_{\rm i}^{-}(z,r,t)$ radiates a two-way, single-pass idler field, whose axial amplitude variation is calculated from the relation

$$\frac{n_{\rm i}}{c}\frac{\partial E_{\rm i}^{\pm}(z,r,t)}{\partial t} \pm \frac{\partial E_{\rm i}^{\pm}(z,r,t)}{\partial z} = -\omega_{\rm i}\mathcal{P}_{\rm i}^{\pm}(z,r,t)/2\varepsilon_0 n_{\rm i}c\,. \quad (4)$$

The $\pm$ distinguishes travelling waves with $\pm k_{{\rm i}j}z$. Since the resonant fields' dynamics occur on a time scale of the order of their high-finesse cavity life-times, the idler experiences a quasi-constant nonlinear source term over its transit of the crystal. We therefore assume that the idler's temporal variations follow those of the resonant waves [11].

With this assumption, and combining (1)–(4), the idler field in the crystal is found to be of the form

$$E_{\rm i}^{\pm}(z,r,t) = \pm\frac{2d_{\rm eff}}{\Delta k n_{\rm i}c}\exp\left(-r^2(w_{\rm p}^{-2}+w_{\rm s}^{-2})\right)E_{\rm s}(t) \times \sum_j\left\{\omega_{\rm i}E_{{\rm p}j}(t)\cos\left(-(\omega_{{\rm i}j}t+\phi_{{\rm i}j}^{\pm}) \pm k_{{\rm i}j}z\right) \times\left(\cos\left(\Delta\phi_j^{\pm} - \Delta k(z_{-l}^{+0})\right) - \cos(\Delta\phi_j^{\pm})\right)\right\}. \quad (5)$$

Here we use a common Δk for every value of $\Delta k_j = k_{{\rm p}j} - k_{\rm s} - k_{{\rm i}j}$ because the laser bandwidth is taken to be much smaller than the parametric gain bandwidth. In the ICSROs described in [1, 3], for example, the spread in Δk_j is less than $0.07\,{\rm cm}^{-1}$. The form of the idler field is not constrained by a resonant cavity so we assume that its transverse variation takes the form of the driving polarisation.

Now since $E_{\rm i}^{\pm}(z,r,t) = 0$ at the start of each pass of the nonlinear crystal, the nonlinear coupling always establishes a phase of $\Delta\phi_j^{\pm} = \pi/2$; i.e. the coupled-wave equations predict that the idler is generated in that phase. Any subsequent perturbation to the phase is rapidly corrected because the idler leaves the cavity after a single pass, and no 'memory' of the perturbation remains in the system. Therefore only the efficient regime of the steady-state solutions can occur. Setting $\Delta\phi_j^{\pm} = \pi/2$ and $\Delta k = 0$, assuming phase matching, simplifies (5) to

$$E_{\rm i}^{\pm}(z,r,t) = \frac{2d_{\rm eff}}{n_{\rm i}c}\exp\left(-r^2(w_{\rm p}^2+w_{\rm s}^2)\right)E_{\rm s}(t)\begin{pmatrix} z \\ l-z\end{pmatrix} \times \sum_j\left\{\omega_{{\rm i}j}E_{{\rm p}j}(t)\cos\left(-(\omega_{{\rm i}j}t+\phi_{{\rm i}j}^{\pm}) \pm k_{{\rm i}j}z\right)\right\}. \quad (6)$$

The envelope of $E_{\rm i}^{\pm}(z,r,t)$ within the crystal increases linearly with $\pm z$.

We subsequently follow the derivation in [11] of the coupled rate equations. We outline this below for comparison with the single-frequency case.

The evolution of the resonant fields is described by the self-consistency equations

$$\dot{E}_{\rm s}(t) + E_{\rm s}(t)/\tau_{\rm s}' = -\omega_{\rm s}C_{\rm s}(t)/2\varepsilon_0 n_{\rm s}^2\,, \quad (7)$$

$$\dot{E}_{{\rm p}j}(t) + E_{{\rm p}j}(t)/\tau_{\rm p}' = -\omega_{{\rm p}j}C_{{\rm p}j}(t)/2\varepsilon_0 n_{\rm p}^2 - \omega_{{\rm p}j}\mathcal{P}_{{\rm laser}\,j}(t)/2\varepsilon_0 n_{\rm p}^2\,. \quad (8)$$

Here $\tau_{\rm s}'$, $\tau_{\rm p}'$ are the signal- and pump-field cavity lifetimes. $\mathcal{P}_{{\rm laser}\,j}$ represents the polarisation in the laser medium which provides optical gain to the system. $C_{\rm s}(t)$, $C_{{\rm p}j}(t)$ are polarisation terms describing the nonlinear medium. They are related to the nonlinear polarisations $\mathcal{P}_x(z,r,t)$, where $x = s$, pj, via the volume integral

$$\mathcal{P}_x(t) = \frac{2}{\pi w_x^2}\frac{2}{L_x}\int_0^l\int_0^{2\pi}\int_0^{\infty}\mathcal{P}_x(z,r,t)\sin(k_x z) \times \exp(-r^2/w_x^2)r\,{\rm d}r\,{\rm d}\varphi\,{\rm d}z = C_x(t)\cos(\omega_x t+\phi_x) + S_x(t)\sin(\omega_x t+\phi_x)\,. \quad (9)$$

Equation (9) projects the nonlinear source terms onto their respective cavity modes. It comprises overlap integrals for both

the transverse and axial variations of $\mathcal{P}_x(z,r,t)$. The axial overlap integral accounts for the varying amplitude of the idler, and the fact that the fields only interact over the length of the crystal.

Combining (1)–(3), (6), and (9) we find the polarisation terms to be

$$C_\mathrm{s}(t) = -\varepsilon_0 l d_\mathrm{eff}^2 \left[2/(1+w_\mathrm{s}^2/\bar{w}_\mathrm{s}^2)\right](l/L_\mathrm{s})E_\mathrm{s}(t) \times \sum_j \omega_{\mathrm{i}j} E_{\mathrm{p}j}(t)^2/cn_\mathrm{i}\,, \tag{10}$$

$$C_{\mathrm{p}j}(t) = -\varepsilon_0 l d_\mathrm{eff}^2 \left[2/(1+w_\mathrm{p}^2/\bar{w}_\mathrm{p}^2)\right](l/L_\mathrm{p})E_{\mathrm{p}j}(t)\omega_{\mathrm{i}j} \times E_\mathrm{s}(t)^2/cn_\mathrm{i}\,, \tag{11}$$

where $\bar{w}_{\mathrm{s,p}}$ is the waist radius of the nonlinear polarisation; it is related to the field waists by

$$1/\bar{w}_{\mathrm{s,p}}^2 = 1/w_\mathrm{i}^2 + 1/w_{\mathrm{p,s}}^2\,. \tag{12}$$

Following a similar argument to [11], we now replace the laser polarisation term in (8) with $G_j E_{\mathrm{p}j}/G_{j-\mathrm{th}}\tau_\mathrm{p}'$, to give

$$\tau_\mathrm{p}'\dot{E}_{\mathrm{p}j} = \left(G_j/G_{j-\mathrm{th}} - 1\right)E_{\mathrm{p}j} - \tau_\mathrm{p}'\omega_{\mathrm{p}j}C_{\mathrm{p}j}/\varepsilon_0 n_\mathrm{p}^2\,. \tag{13}$$

G_j is the saturated gain associated with the jth laser mode ($\sum G_j \propto$ laser population inversion), while $G_{j-\mathrm{th}}$ is the threshold gain required for laser oscillation.

We now have all of the necessary polarisation terms to form the coupled rate equations. Before proceeding to the steady-state and transient analyses, we simplify the equations by introducing a similar dimensionless notation to that in [11]. The resonant fields are first re-expressed as photon flows:

$$\mathcal{F}_\mathrm{s} = n_\mathrm{s} c\varepsilon_0 E_\mathrm{s}^2 \pi w_\mathrm{s}^2/4\hbar\omega_\mathrm{s}\,,$$
$$\mathcal{F}_{\mathrm{p}j} = n_\mathrm{p} c\varepsilon_0 E_{\mathrm{p}j}^2 \pi w_\mathrm{p}^2/4\hbar\omega_{\mathrm{p}j} \tag{14}$$

and we note from (7) and (10) that for the signal field to experience gain, the laser photon flow must exceed the threshold value

$$\left[\sum_j \mathcal{F}_{\mathrm{p}j}\right]_\mathrm{th} = \frac{n_\mathrm{p} n_\mathrm{s}^2 n_\mathrm{i} c^2 \varepsilon_0 L_\mathrm{s}}{\hbar\omega_\mathrm{p}\omega_\mathrm{s}\omega_\mathrm{i}\tau_\mathrm{s}' d_\mathrm{eff}^2 l^2} \frac{\pi(w_\mathrm{s}^2 + w_\mathrm{p}^2)}{2}\,. \tag{15}$$

The threshold value on the right of (15) is identical to that of (27) in [11] when $\alpha_\mathrm{id} = 0$. However, now the threshold must be attained by the total photon flow of all of the laser modes. So long as the laser bandwidth is sufficiently small that one may consider that all nonlinear processes are phase matched, then the multi-mode laser provides the same gain as a single-frequency laser of the same total power [23].

We now define a normalised gain, signal power, and laser power by

$$N_j = G_j/G_{j-\mathrm{th}}\,, \tag{16}$$
$$P_\mathrm{s} = \mathcal{F}_\mathrm{s}/\left[\sum \mathcal{F}_{\mathrm{p}j}\right]_\mathrm{th}\,, \tag{17}$$
$$P_{\mathrm{p}j} = \mathcal{F}_{\mathrm{p}j}/\left[\sum \mathcal{F}_{\mathrm{p}j}\right]_\mathrm{th}\,. \tag{18}$$

After multiplying (7) by E_s and (8) by $E_{\mathrm{p}j}$, the coupled equations are given by

$$\tau_\mathrm{s}\dot{P}_\mathrm{s} = P_\mathrm{s}\left(\sum_j P_{\mathrm{p}j} - 1\right)\,, \tag{19}$$
$$\tau_\mathrm{p}\dot{P}_{\mathrm{p}j} = P_{\mathrm{p}j}\left(N_j - 1 - FP_\mathrm{s}\right)\,, \tag{20}$$

where $F = \tau_\mathrm{p}' n_\mathrm{s} L_\mathrm{s}/\tau_\mathrm{s}' n_\mathrm{p} L_\mathrm{p}$ is the ratio between the laser and signal cavity finesses; τ_s, τ_p are the signal and pump photon lifetimes which are twice their respective field values.

Finally, we add the evolution equation for the saturated laser gain, which may be derived from the Bloch equations [11]:

$$\tau_\mathrm{u}\dot{N}_j = \sigma_j - N_j\left(1 + xP_{\mathrm{p}j} + x\mu\sum_{k\neq j} P_{\mathrm{p}k}\right)\,. \tag{21}$$

τ_u is the upper-state lifetime and σ_j is the number of times the jth laser mode is pumped above threshold ($\sigma_j \propto$ unsaturated gain). x is a saturation parameter, defined as

$$x = \left[\sum \mathcal{F}_{\mathrm{p}j}\right]_\mathrm{th}/\mathcal{F}_\mathrm{sat}\,, \tag{22}$$

where $\mathcal{F}_\mathrm{sat}$ is the laser saturation photon-flow. We include cross-saturation between pairs of laser modes through the coefficient $\mu < 1$. Equation (21) is identical in form to that used by Baer in [9]. He found that the cross-saturation terms, which are due to partial inhomogeneous broadening, are essential to a description of a multi-mode laser with intracavity frequency doubling. The inclusion of these terms allows a fair comparison between Baer's model and the present work. We now proceed to analyse the steady-state and transients of (19)–(21).

3 Steady-state power characteristics

We consider first the case of a single-frequency laser field. Setting time derivatives to zero, (19)–(21) yield the steady-state solution for operation above the OPO threshold, $\sigma \geq \sigma_{\mathrm{th-OPO}} = 1 + x$, as

$$P_\mathrm{p}^0 = 1, \quad N^0 = \sigma/(1+x), \quad P_\mathrm{s}^0(N^0 - 1)/F\,. \tag{23}$$

This is shown graphically in region III of Fig. 2. Above the OPO threshold, we find that the laser field is clamped to its threshold value, independent of the level of external pumping. Power is down-converted into the signal and idler fields which increase linearly with external pumping. The clamped laser field limits the degree to which the laser gain is saturated; the gain now increases linearly with external pump power. Below OPO threshold, the ICSRO operates as a conventional laser.

We next consider the steady-state operation including a multi-frequency laser field. The general steady-state solu-

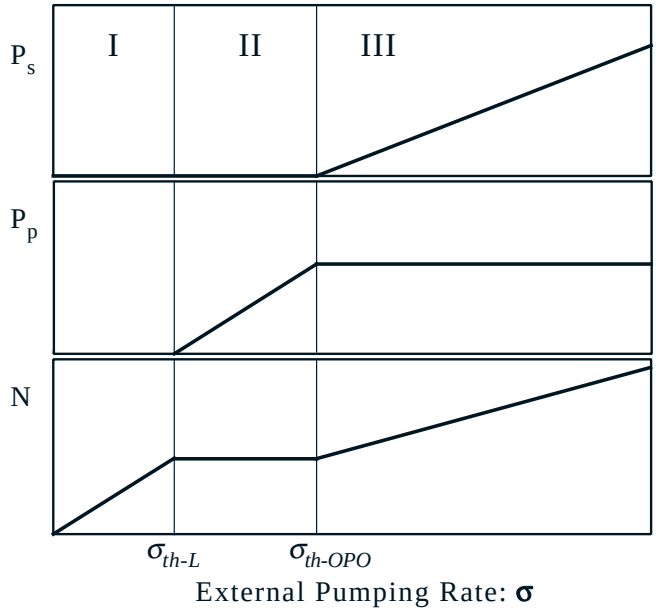

Fig. 2. Steady-state operation of signal power P_s, laser-pump power P_p, and saturated gain N

tion of equations (19)–(21) with M axial laser modes is:

$$P_{pj}^0 = \sigma_j / \sum_j \sigma_j + (1 + x\mu) \times \left(M\sigma_j - \sum_j \sigma_j \right) \Big/ \left(x(1-\mu) \sum_j \sigma_j \right) ,$$
$$N_j^0 = \sum_j \sigma_j / \{M + x\,(1 + \mu(M-1))\} ,$$
$$P_s^0 = (N_j^0 - 1)/F . \qquad (24)$$

Now the total laser power $\sum_j P_{pj}^0$ is clamped at the OPO threshold level, as shown previously in (15) and experimentally in [1]. The laser gain has a common value for every laser mode and, together with the down-converted signal, increases linearly with the total external pumping power.

From the requirement that $P_{pj}^0 \geq 0$, we find that each of the M modes must satisfy

$$\sigma_j \geq (\sigma_j)_{th-L} = N_j^0(1 + x\mu) = 1 + x\mu \sum_{k \neq j} P_{pk}^0 + FP_s^0(1 + x\mu) ; \qquad (25)$$

a new threshold condition which includes the parametric loss to individual modes (in the absence of parametric loss, the laser has a threshold of $(\sigma_j)_{th-L} = 1 + x\mu \sum_{k \neq j} P_{pk}^0$). Now the gain to an individual mode must exceed the nonlinear loss presented by the signal field (whose magnitude depends on the total laser gain) as well as the parasitic cavity loss and gain cross-saturation effects. To achieve oscillation, the gain to a given laser mode must now be greater than a fraction $[1 + x\mu]/[M(1 + x\mu) + x(1 - \mu)]$ of the total laser gain.

The consequence of (25) is to narrow the laser linewidth when above OPO threshold. For some modes in the low-gain wings of the laser gain profile may not be able to tolerate the additional loss $FP_s^0(1 + x\mu)$. These modes, which were present when below OPO threshold, can no longer oscillate. An estimate of the degree of narrowing would require an analysis of the spatial-hole-burning in the medium to determine the distribution of σ_j, but we can note here that the allowed deviation from the mean σ_j is inversely proportional to the number of oscillating modes.

4 Power optimisation

Optimisation of the down-converted power of the ICSRO was first considered by Tran-Ba-Chu and Broyer [17]. They showed that, under optimum nonlinear coupling, 100% of the potentially extractable laser power could be down-converted. In this section we derive simple expressions, involving the experimentally measurable quantities of laser and OPO thresholds, to describe optimisation of the idler and signal outputs.

Combining (17) and (22)–(23) (for the case of a single-frequency laser), we obtain an expression for the signal photon-flow inside the OPO cavity:

$$\mathcal{F}_s = \frac{\mathcal{F}_{sat}}{\alpha_s} \left(\frac{\sigma}{\sigma_{th-OPO}} - 1 \right) \alpha_p (\sigma_{th-OPO} - \sigma_{th-L}) , \qquad (26)$$

where we have made the substitution $F = \alpha_s/\alpha_p$; α_s, α_p are the round-trip photon losses in the signal and pump cavities. $\alpha_p\sigma_{th-L}$ and $\alpha_p\sigma_{th-OPO}$ are the round-trip gains required to achieve laser and OPO thresholds, respectively.

In the steady-state, the round-trip photon losses from the signal and idler fields are equal. Thus the idler photon-flow output is

$$(\mathcal{F}_i)_{out} = \alpha_s \mathcal{F}_s = \mathcal{F}_{sat} \left(\frac{\sigma}{\sigma_{th-OPO}} - 1 \right) \alpha_p (\sigma_{th-OPO} - \sigma_{th-L}) . \qquad (27)$$

Now we wish to find the optimum value of σ_{th-OPO} for a given pumping rate σ. This may be done by solving the equation

$$\frac{\partial (\mathcal{F}_i)_{out}}{\partial \sigma_{th-OPO}} = 0 . \qquad (28)$$

We thereby find that the idler power for a given pumping rate σ is greatest when

$$\sigma_{th-OPO} = \sqrt{\sigma_{th-L}\sigma} . \qquad (29)$$

That is when the OPO threshold is the geometrical mean of the laser threshold and the applied external pumping rate. Substitution of (29) into (27) gives

$$(\mathcal{F}_i)_{out}^{max} = \mathcal{F}_{sat}\alpha_p(\sqrt{\sigma} - \sqrt{\sigma_{th-L}})^2 \equiv (\mathcal{F}_p)_{out} , \qquad (30)$$

which is the familiar expression for the output power of a laser $(\mathcal{F}_p)_{out}$ when subject to optimum output-coupling. Therefore when (29) holds, the OPO is 100% efficient. Figure 3 plots the ratio of $(\mathcal{F}_i)_{out}$ to $(\mathcal{F}_p)_{out}$ against the external pumping rate. Once above threshold, the efficiency rapidly rises to 100% before gradually tailing off as the OPO over-couples the laser field. By arranging the OPO threshold to satisfy (29), the idler output power may be optimised at any pump power.

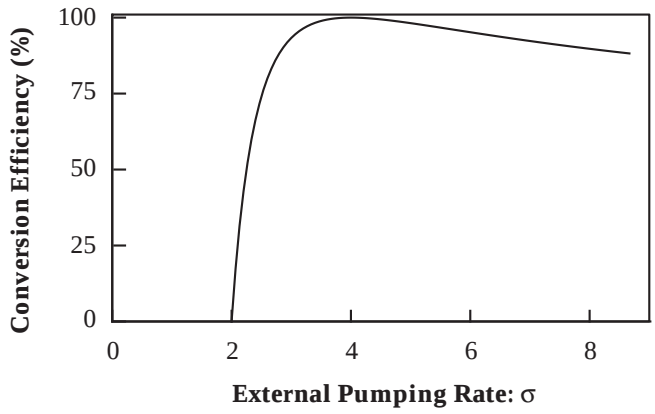

Fig. 3. Down-conversion efficiency expressed as percentage of extractable laser power

We have repeated the derivation from (6) onwards with $\Delta k \neq 0$, and find that (26) still holds, but now with $\sigma_{\text{th-OPO}} = 1 + x/\,\text{sinc}^2(\Delta kl)$. It follows that (29) and (30) are true for any Δk. The single-frequency analysis (26)–(30) may easily be extended to the multi-mode steady-state of (24). Again, (29) and (30) are true, assuming a common value of Δk for all modes, but where σ, $\sigma_{\text{th-L}}$, $\sigma_{\text{th-OPO}}$ are now replaced by $\sum \sigma_j$, $(\sum \sigma_j)_{\text{th-L}}$, $(\sum \sigma_j)_{\text{th-OPO}}$.

To optimise the signal power, we must divide the signal round-trip loss into a parasitic loss α_{sp} and an output coupling loss α_{so}. The signal output photon-flux may then be re-expressed as

$$(\mathcal{F}_{\text{s}})_{\text{out}} = \alpha_{\text{so}}\mathcal{F}_{\text{s}} = \alpha_{\text{so}}\alpha_{\text{p}}K\left(\frac{\sigma}{1+(\alpha_{\text{so}}+\alpha_{\text{sp}})K/\mathcal{F}_{\text{sat}}}-1\right), \tag{31}$$

where we have combined equations (17), (22), and (23) and defined

$$(\mathcal{F}_{\text{p}})_{\text{th}} = \alpha_{\text{s}}K\,, \tag{32}$$

since we note that $\alpha_{\text{s}} \propto 1/\tau_{\text{s}}'$. As before, we optimise the signal output by solving the equation

$$\frac{\partial(\mathcal{F}_{\text{s}})_{\text{out}}}{\partial\alpha_{\text{so}}} = 0\,. \tag{33}$$

We find that the signal power, for a given pumping rate σ, is greatest when

$$\sigma_{\text{th-OPO}} = \sqrt{(\sigma_{\text{th-OPO}})_{\text{min}}\sigma}\,. \tag{34}$$

$(\sigma_{\text{th-OPO}})_{\text{min}}$ is the OPO threshold in the absence of signal output coupling.

It is obvious that the signal and idler can only be simultaneously optimised in the limit when $(\sigma_{\text{th-OPO}})_{\text{min}} \approx \sigma_{\text{th-L}}$. Most applications, of course, will only require one of the two wavelengths, so we propose three optimisation schemes for the ICSRO.

4.1 Idler power

To optimise the idler power one sets the OPO threshold pump rate to satisfy (29). Since output coupling of the signal is not important, this may be done by either choosing the appropriate length of nonlinear crystal or, if power damage is an issue, by increasing the beam waist in the crystal [17].

4.2 Signal power

To optimise the signal power one minimises the value of $(\sigma_{\text{th-OPO}})_{\text{min}}$, so that the OPO may be pumped as high above threshold as possible, then open up the output coupling so as to satisfy (34).

4.3 Total power

As with the signal optimisation, one minimises the value of $(\sigma_{\text{th-OPO}})_{\text{min}}$ by using as strong a nonlinear coupling as possible. But now the output coupling should be increased to raise the threshold value to satisfy (29). This optimises the idler power, while setting the signal output on the gradual decline in efficiency due to over-coupling.

5 Power stability analysis

While a numerical analysis of the rate equations such as that in [9] can show directly the presence and form of fluctuations, an indirect analytical approach can be of significant use as a probe for the presence of instability [8, 10]. Our approach is to use Liapunov's direct method [24] to test whether the system (19)–(21) can exhibit the instabilities which may lead to large-scale power fluctuations. For comparison with the other intracavity systems of [8] and [9, 10], we state the results of a Liapunov analysis of each.

We first consider the steady-state solutions (23). Re-expressing (19)–(21) in terms of deviations δP_{p}, δP_{s}, δN from P_{p}^0, P_{s}^0, N^0 we obtain:

$$\tau_{\text{s}}\delta\dot{P}_{\text{s}} = \delta P_{\text{p}}(\delta P_{\text{s}} + P_{\text{s}}^0)\,, \tag{35}$$

$$\tau_{\text{p}}\delta\dot{P}_{\text{p}} = (\delta P_{\text{p}} + 1)(\delta N - F\delta P_{\text{s}})\,, \tag{36}$$

$$\tau_{\text{u}}\delta\dot{N} = -\delta N(1+x) - x\delta P_{\text{p}}(\delta N + N^0)\,. \tag{37}$$

We now form a Liapunov function for the system (35)–(37). The Liapunov function $V(\delta P_{\text{p}}, \delta P_{\text{s}}, \delta N)$ is a scalar function analogous to the total energy of a mechanical system. It has the properties [24] that: (a) $V(\delta P_{\text{p}}, \delta P_{\text{s}}, \delta N)$, and its first partial derivatives, are continuous within some region Ω about the origin, (b) $V = 0$ at the origin and elsewhere in Ω $V > 0$, and (c) $\dot{V} \leq 0$ in Ω.

By neglecting the spontaneous emission term in (37), and then integrating (35)–(37) with respect to time, we identify a Liapunov function for this system as

$$V = \tau_{\text{p}}\left\{\delta P_{\text{p}} - P_{\text{p}}^0\ln(P_{\text{p}}/P_{\text{p}}^0)\right\} + F\tau_{\text{s}}\left\{\delta P_{\text{s}} - P_{\text{s}}^0\ln(P_{\text{s}}/P_{\text{s}}^0)\right\} + \tau_{\text{u}}\left\{\delta N - N^0\ln(N/N^0)\right\}/x\,, \tag{38}$$

the general form of which is shown in Fig. 4. Provided $\sigma \geq 1 + x$ (the OPO threshold condition) then $V \geq 0$, and

takes a minimum value of zero at the origin of the δP_p, δP_s, δN phase-space (the steady-state solution). Taking the time derivative of (38) yields

$$\dot{V} = -(1+x)\delta N^2/x\tau_p(N^0+\delta N)\ . \tag{39}$$

Since $\delta N \geq -N^0$, (39) is always negative. This implies that as the system evolves with time, the magnitude of V decreases to its minimum value; the system always settles to the steady state. We may therefore infer that, given $\sigma \geq 1+x$, the cw efficient regime of the ICSRO is completely stable against any perturbation, and that no repetitively pulsing mode exists.

This result may be compared with the Liapunov function for the ICDRO:

$$2V_{DRO} = \delta\dot{E}_3^2 + \delta(\phi_3-\phi_1-\phi_2)^2 + \omega_3\kappa^2(\omega_1E_2^2+\omega_2E_1^2)\delta E_3^2\ , \tag{40}$$

$$\dot{V}_{DRO} = (g_0-\alpha_3-3g_0\beta E_3^2)\delta\dot{E}_3^2 + \kappa(\phi_3-\phi_1-\phi_2)^2 \times (\omega_3E_1^2E_2^2-(\omega_1E_2^2+\omega_2E_1^2)E_3^2)\big/E_1E_2E_3\ , \tag{41}$$

where δE_3, $\delta(\phi_3-\phi_1-\phi_2)$ are deviations from their respective steady-state values, and all other notation is as defined in [8] with $\alpha_1=\alpha_2$. For $V_{DRO}\geq 0$ and $\dot{V}_{DRO}\leq 0$ we require

$$(g_0-\alpha_3) > g_0\beta E_3^2\ , \tag{42a}$$

$$(g_0-\alpha_1-\alpha_2-\alpha_3) < g_0\beta E_3^2\ , \tag{42b}$$

$$(g_0-\alpha_3) < 3g_0\beta E_3^2 \tag{42c}$$

to be satisfied. These are the stability conditions of equations (30), (31), and (32) in [8]; if not fulfilled, the system will be either (a) below threshold, (b) in the inefficient regime, or (c) exhibit large amplitude fluctuations.

Oshman and Harris qualitatively explain the pulsing mechanism in the ICDRO when (42c) is not satisfied. They show that the build-up rate, at high intracavity pump powers, of the signal and idler can be sufficiently rapid that it exceeds the cavity decay rate of the pump. While at low pump powers, the laser field may build up much faster than the down-converted fields. This causes repeated overshooting of the steady-state levels, yielding a train of pulses. The ICSRO does not exhibit this behaviour because the non-resonant idler acts as a regulator to changes in the resonant fields. It produces a more rapid response in one resonant field to a change in the other, which may be seen in the quadratic, rather than linear dependence of the other resonant field in (10) and (11). This action prevents the positive feedback which causes pulsing in the ICDRO.

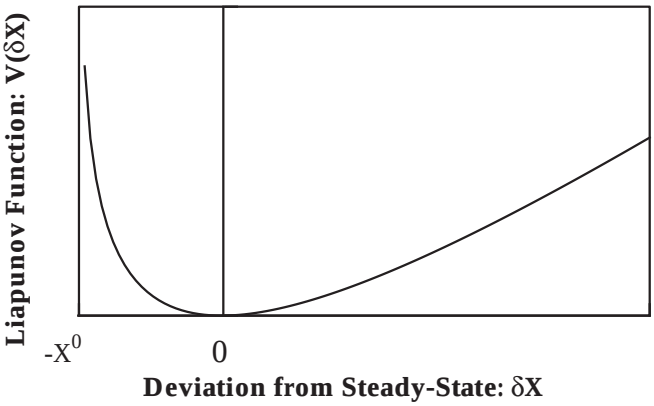

Fig. 4. General form of Liapunov function (38)

Next we analyse the multi-frequency laser operation in (24). Following the analysis of multi-frequency intracavity up-conversion [10], we simplify our stability analysis by setting $\sigma_j=\sigma$. We consider only the linear terms in the deviations from the steady state, given that for small perturbations the system is dominated by these linear terms. Such a linear analysis yields a parabolic Liapunov function:

$$V_M = \tau_p\left\{\mu\left(\sum_j \delta P_{pj}\right)^2 + (1-\mu)\sum_j \delta P_{pj}^2\right\}\Big/P_{pj}^0 + \tau_sF\,(1+\mu(M-1))\,\delta P_s^2/\delta P_s^0 + \tau_u\sum_j \delta N_j^2\big/xN_j^0\ . \tag{43}$$

The time derivative of (43) is

$$\dot{V}_M = -2\delta N_j^2\sigma/x{N_j^0}^2\ . \tag{44}$$

As for the single-frequency case $V_M\geq 0$ and $\dot{V}_M\leq 0$. So linear asymptotic stability is ensured when the ICSRO is pumped above threshold.

We have extended this analysis to include multiple signal frequencies, which interact independently with the pump field. As for the single-frequency signal case, we find no evidence of an unstable pulsing mode. However, the steady-state solution tends to collapse to the single-frequency signal case if any one mode experiences a lower threshold than the others. This is in agreement with the experimental evidence in [1, 3]. Additionally, we have shown that the use of étalons in the OPO cavity can ensure single-frequency signal operation [3]. We thus conclude that a single-frequency signal field is a sufficient, practical condition for stable ICSRO operation.

This result is quite different from that of intracavity up-conversion, where other requirements for stability exist [10], giving rise to the so-called "green problem". The Liapunov function and its time derivative for that system are

$$V_{SHG} = \tau_c\sum\delta\dot{I}_k^2/2I_s + G_s(1-\beta-g\varepsilon\gamma/G_s^2)\sum\delta I_k^2/2\tau_f + G_s(\beta+2g\varepsilon\gamma/G_s^2)\left[\sum\delta I_k\right]^2/2\tau_f\ , \tag{45}$$

$$\dot{V}_{SHG} = (g\varepsilon-\tau_c\gamma/\tau_fI_sG_s)\sum\delta\dot{I}_k^2 - 2g\varepsilon\left[\sum\delta\dot{I}_k\right]^2\ , \tag{46}$$

where $\delta I_k = I_k - I_s$ and all other notation is as defined in [10]. Clearly, for $V_{SHG}\geq 0$ and $\dot{V}_{SHG}\leq 0$ we require

$$g < \tau_c\gamma/\tau_f\varepsilon I_sG_s\ , \tag{47a}$$

$$g < (1-\beta)G_s^2/\varepsilon\gamma \tag{47b}$$

to be satisfied. These are the stability conditions of (9) and (10) in [10]; if not fulfilled, the system will exhibit large amplitude fluctuations.

The erratic pulsing behaviour of the green problem results from a combination of sum-frequency-mixing and cross-saturation of different axial modes. While the ICSRO also

exhibits gain cross-saturation, it does not feature any direct nonlinear coupling of laser modes. Instead each laser frequency interacts only with a common signal mode, which may then interact with another laser mode. So it appears that the signal field acts as a buffer between laser modes to prevent unstable fluctuations.

It is important to highlight that for the case of the multimode laser we have demonstrated stability only to small perturbations, and not (as with the single-frequency case) to any perturbation. For a more general statement of stability it will be necessary to employ either a numerical or experimental investigation. Nevertheless we note that the other intracavity systems which do show fluctuations are unstable even to small perturbations. The contrasting linear stability of the multi-laser-mode-, and complete stability of the single-laser-mode-, ICSROs show promise for general stability in the multi-mode system.

6 Transient power analysis: relaxation oscillations

Having established that the ICSRO is stable for any pumping level, it is now useful to quantify the practical extent of that stability. For we have so far shown that the system will always evolve towards the steady state in response to a perturbation, but not the manner of the evolution. If the system takes longer to settle than the time between perturbations, it will never reach a true steady state; different applications of the system will require different degrees of amplitude stability.

So to address this issue of practical stability, we study the transient dynamics of the ICSRO. We consider only a system with the relatively simple dynamics of a single-frequency laser-pump field. This allows the derivation of quite simple expressions which describe the characteristic time scales of the transients.

We first examine the case where the laser upper-state lifetime is small, and make the approximation that $\tau_u \approx 0$. Equations (20) and (21) are reduced to

$$\tau_p \dot{P}_p = P_p \left(\frac{\sigma}{1+xP_p} - 1 - FP_s \right) . \tag{48}$$

We now re-express (19) and (48) in terms of perturbations δP_p, δP_s from P_p^0, P_s^0:

$$\tau_s \delta\dot{P}_s = \delta P_p \frac{1}{F} \left(\frac{\sigma}{1+x} - 1 \right) + O(\delta P^2) , \tag{49}$$

$$\tau_p \delta\dot{P}_p = -\frac{x\sigma}{(1+x)^2} \delta P_p - F\delta P_s + O(\delta P^2) , \tag{50}$$

where $O(\delta P^2)$ includes all terms involving products of δP_p, δP_s.

For small perturbations, where equations (49) and (50) are dominated by the terms linear in δP_p, δP_s, the system shows relaxation oscillations described by

$$\begin{aligned} \delta P &\propto \exp(-\gamma t)\cos(\omega t + \varphi) , \\ \gamma &= \frac{\sigma}{2\tau_p \sigma_{\text{th-OPO}}} \left(1 - \frac{\sigma_{\text{th-L}}}{\sigma_{\text{th-OPO}}} \right) \\ \omega &= \sqrt{\frac{1}{\tau_s \tau_p} \left(\frac{\sigma}{\sigma_{\text{th-OPO}}} - 1 \right) - \gamma^2} , \end{aligned} \tag{51}$$

when $(\sigma/\sigma_{\text{th-OPO}} - 1)/\tau_s\tau_p > \gamma^2$. As with the optimisation conditions, we choose to express γ, ω explicitly in terms of the experimentally measurable thresholds. These relaxation oscillations arise from the dynamics of the SRO alone since the approximation $\tau_u \approx 0$ disallows any laser relaxation oscillations. Equation (51) describes the dynamics of dye-laser based ICSROs such as the one described in [2] where usually $\tau_u \ll \tau_s, \tau_p$.

The form of (51) is similar to that for laser relaxation oscillations where the lifetimes τ_p, τ_s in the ICSRO take the place of τ_u, τ_p in the laser. The expressions differ with the extra factor in γ in (51) which depends on the ratio of laser and OPO thresholds. The relaxation oscillations in an ICSRO also differ from those in an external-cavity pump-enhanced OPO, originally proposed in [25] and recently demonstrated in [26]. In the external-cavity OPO γ is independent of pumping level and depends solely on τ_p.

We now repeat our analysis, this time allowing for independent dynamics in the laser population inversion. First we rewrite (20) and (21) in terms of linear perturbations δP_p, δP_s, δN from P_p^0, P_s^0, N^0:

$$\tau_p \frac{\partial \delta P_p}{\partial t} = \delta N - F\delta P_s + O(\delta X^2) , \tag{52}$$

$$\tau_u \frac{\partial \delta N}{\partial t} = -\frac{x\sigma}{1+x} \delta P_p - (1+x)\delta N + O(\delta X^2) , \tag{53}$$

where $O(\delta X^2)$ includes all terms involving products of δP_p, δP_s, δN.

The linear terms in (49), (52), and (53) may be combined to form a third-order differential equation with solution

$$\delta P = \sum_{r=1}^{3} \alpha_r \exp(\lambda_r t) , \tag{54}$$

where λ_r are the roots of the cubic

$$\begin{aligned} 0 = {} & \tau_p\tau_u\tau_s\lambda^3 + (1+x)\tau_p\tau_s\lambda^2 \\ & + \frac{\tau_s x\sigma + \tau_u(\sigma - 1 - x)}{1+x}\lambda + \sigma - 1 - x . \end{aligned} \tag{55}$$

In general the solution will be a superposition of an exponential decay and a pair of quadrature-phased, exponentially damped sinusoidal oscillations. For the special case $\tau_u \approx 0$, (54) and (55) reduce to the OPO oscillations of equation (51), whereas for $\tau_s \gg \tau_u$, τ_p (54) becomes

$$\begin{aligned} \delta P &\propto \exp(-\gamma t)\cos(\omega t + \varphi) , \\ \gamma &= \frac{\sigma_{\text{th-OPO}}}{2\sigma_{\text{th-L}}\tau_u} , \\ \omega &= \sqrt{\frac{\sigma_{\text{th-OPO}}/\sigma_{\text{th-L}} - 1}{\tau_u\tau_p} \frac{\sigma}{\sigma_{\text{th-OPO}}} + \frac{1}{\tau_s\tau_p} \left(\frac{\sigma}{\sigma_{\text{th-OPO}}} - 1 \right) - \gamma^2} \end{aligned} \tag{56}$$

which describes relaxation oscillations which are dominated by the laser's dynamics. For $\sigma = \sigma_{\text{th-OPO}}$ (56) reduces to the standard expression for laser relaxation oscillations. At higher pumping levels, the pump-clamping effect controls the damping term, while the frequency combines terms characteristic of both the laser and OPO oscillations.

Equations (54) and (55) may be used to observe the transition from laser-dominated to OPO-dominated relaxation oscillations. Figure 5 shows the characteristics of the underdamped component of (54), where we have normalised the time constants to τ_s. The top graph shows damping coefficients $\gamma\tau_s$ for different values of τ_u/τ_s, as τ_p/τ_s is varied; the bottom graph shows the corresponding oscillation frequencies $\omega\tau_s$. The curves represent relaxation oscillations for ICSROs when pumped at a level for optimum down-conversion. From (22) we note that x is related to the laser saturation flow $\mathcal{F}_{sat} \propto 1/\tau_u$; we arbitrarily choose to set $x = \tau_u/\tau_s$.

For small values of τ_p/τ_s the damping depends only on τ_u/τ_s which is characteristic of laser oscillations. The magnitude of the damping term will be discussed below. For large values of τ_p/τ_s, we find that $\gamma \propto 1/\tau_p$, as in (51). The change in the oscillation frequency is most obvious for $\tau_u/\tau_s = 0.1$, where there is an over-damped region of operation between the laser- and OPO-dominated oscillations. For other values of τ_u/τ_s the difference in $\omega\tau_s$ between (51) and (56) is clear as the system passes through its transition.

We now analyse numerically the stability of practical systems based on Ti:sapphire and Nd:YVO_4 lasers. Figure 6 shows the relaxation oscillations of a Ti:sapphire-based system similar to [1], where the transients were calculated using (49), (52), and (53) with $M = 1$, for a pumping level of twice OPO threshold. The laser and OPO thresholds are 1 W and 4 W of argon-ion laser power, respectively; $\tau_u = 3.2\,\mu s$, $\tau_s = 0.3\,\mu s$, and $\tau_p = 0.2\,\mu s$. The damping and frequency for the ICSRO are found to be $\gamma = 0.13\,\mu s$, $\omega = 2.3\,\text{rad}\,\mu s^{-1}$. This damping time is significantly longer than that of the Ti:sapphire laser, but is still rapid compared with Nd-based lasers.

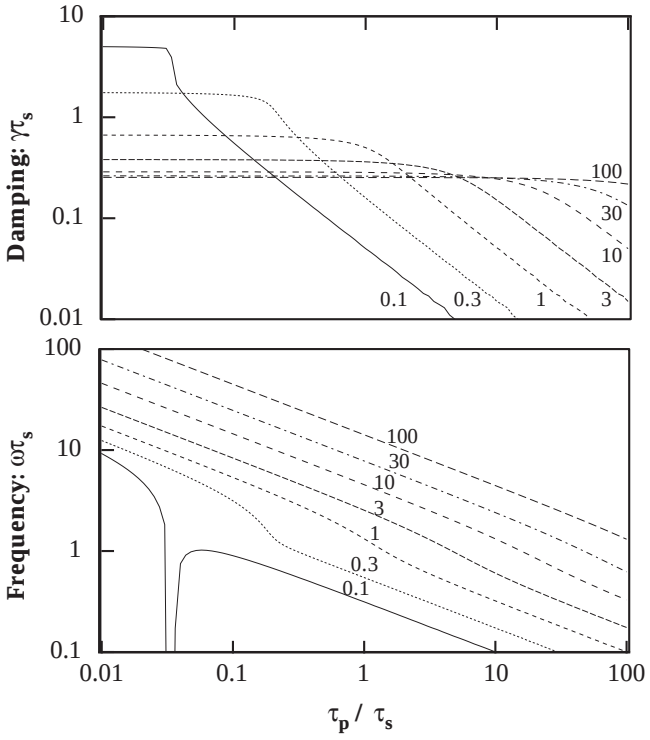

Fig. 5. Damping and frequency of relaxation oscillations for different values of τ_u/τ_s

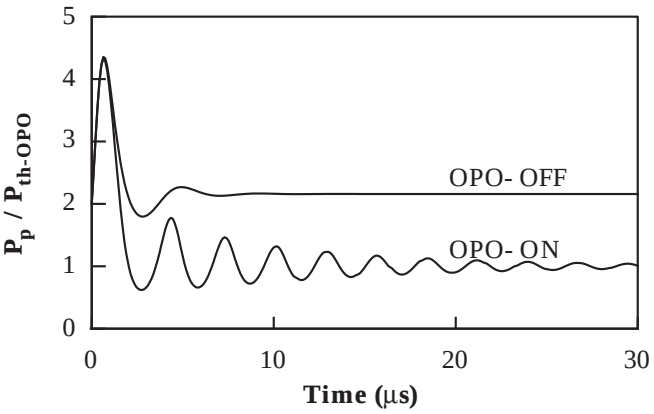

Fig. 6. Calculated transients for Ti:sapphire-based ICSRO

Figure 7 shows the damping time-constant of the relaxation oscillations for a Nd:YVO_4 system, similar to the Nd-based ICSROs in [4, 5], which is calculated from (55). This system has a laser threshold of 0.5 W and an OPO threshold of 4 W; $\tau_u = 98\,\mu s$, $\tau_s = 1\,\mu s$ and $\tau_p = 1\,\mu s$. The damping time-constants for both the basic laser, and the ICSRO are shown, together with the damping predicted from the approximation of (56). As the diode pumping level increases, we find that while the laser damping time drops, the ICSRO damping time rises from its OPO threshold value. The ICSRO curve diverges from the predicted damping of (56) because the approximation $\tau_s \gg \tau_p, \tau_u$ does not hold. Instead we find that, at high powers, the damping time settles to a level roughly ten times longer than that of the laser at OPO threshold. In practice, however, this is still only $\approx 100\,\mu s$ since the laser is pumped well above threshold.

Figure 8 shows the damping times for this system at high pump powers as we now increase τ_s. These clearly converge to the level predicted in (56) as τ_s approaches τ_u. We find that the value of τ_p has little effect on the damping, in agreement with Fig. 5. So the expression for γ in (56) represents the strongest damping that may be achieved, by optimising τ_s and τ_p, in ICSROs based on most solid-state lasers. A direct solution of (55), meanwhile, is more useful for predicting experimental transients of specific ICSRO systems.

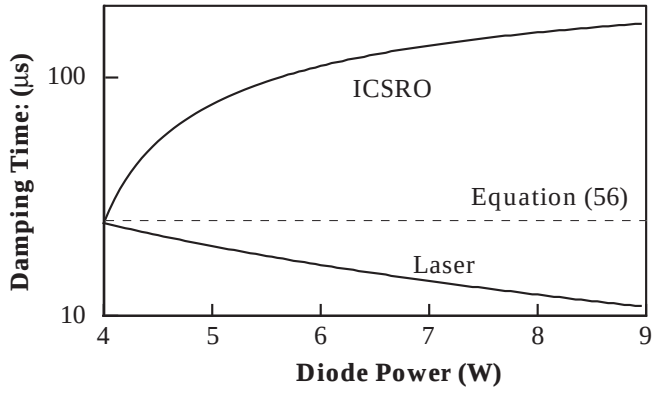

Fig. 7. Relaxation oscillation damping in a Nd:YVO_4-based ICSRO

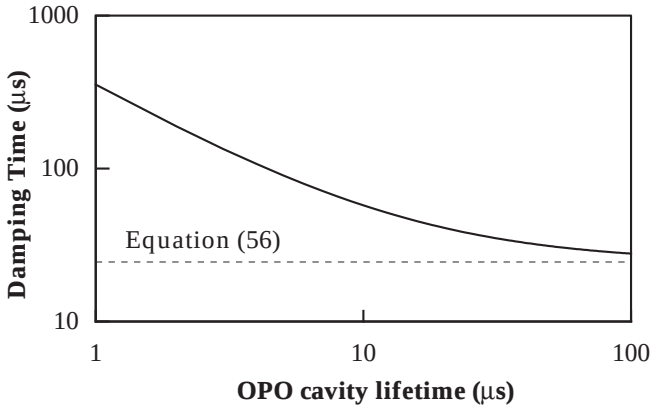

Fig. 8. Dependence of relaxation damping with τ_s

Naturally, to optimise the power stability of the ICSRO it is most important to minimise the size and frequency of the perturbations. These may arise through axial mode-hopping, or fluctuations in the transverse modes (arising from the spatial variation in gains and losses within the system). Such perturbations may be minimised through careful mechanical and optical design of the ICSRO cavities. Stability may then be further optimised by maximising the system's response to the perturbation. We find that this may be done principally by maximising the signal cavity lifetime, particularly when using Nd-based lasers.

7 Conclusions

We have described the steady-state and transient power characteristics of cw ICSROs. The operation characteristics of recently demonstrated ICSROs are reviewed, and a rate-equation model has been derived which forms the basis for a steady-state and transient analysis. The model embodies the key characteristics of the experimental systems [1–7] of multi-frequency, cross-saturated laser fields which couple through a single-frequency signal.

The steady-state behaviour of the device is detailed. In addition to the steady-state features previously reported from theory and experiment, we find a new threshold condition for individual laser modes which causes a narrowing of the laser linewidth. We derive the conditions under which signal and idler output powers are maximised. With these simple expressions, we propose schemes for optimising ICSRO output.

A Liapunov analysis tests the high-power stability of the system. We find that ICSROs do not suffer from the problems of instability which are characteristic of other intracavity frequency-mixing schemes, and as such represent practical continuous-wave sources capable of high output powers and conversion efficiencies. Finally, we quantify the level of practical stability through an analysis of the novel transient behaviour of the ICSRO. Equations describing relaxation oscillations are derived. We find that, to maximise the power stability, the signal cavity lifetime should be made as large as possible.

Acknowledgements. G.A.T. acknowledges personal support from the Carnegie Trust for the Universities of Scotland. M.E. gratefully acknowledges the Royal Society of London for the provision of a University Research Fellowship.

References

1. F.G. Colville, M.H. Dunn, M. Ebrahimzadeh: Opt. Lett. **22**, 75 (1997); M.H. Dunn, M. Ebrahimzadeh: IQEC 96 (1996)
2. M.E. Klein, M. Scheidt, K.-J. Boller, R. Wallenstein: CLEO Europe 1996 paper CTu 01
3. F.G. Colville, T.J. Edwards, G.A. Turnbull, M.H. Dunn, M. Ebrahimzadeh: Conference on Lasers and Electro-Optics, Vol. 11 of 1997 OSA Technical Digest Series (Optical Society of America, Washington, DC 1997) p. 341;
T.J. Edwards, G.A. Turnbull, M.H. Dunn, M. Ebrahimzadeh, F.G. Colville: Appl. Phys. Lett. **72**, 1527 (1998)
4. L.P. Gonzalez, V. Dominic, L.E. Myers, R.C. Eckhardt: Conference on Lasers and Electro-Optics, Vol. 11 of 1997 OSA Technical Digest Series (Optical Society of America, Washington, DC 1997) p. 18
5. F.G. Colville, G.J. Hall, B.T. McGuckin, R.B. Dennis, T.J. Edwards, G.A. Turnbull, M.H. Dunn, M. Ebrahimzadeh: Laser '97, Munich
6. G.A. Turnbull, T.J. Edwards, M.H. Dunn, M. Ebrahimzadeh: Electron. Lett. **33**, 1817 (1997)
7. T.J. Edwards, G.A. Turnbull, M.H. Dunn, M. Ebrahimzadeh, H. Karlsson, G. Arvidsson, F. Laurell: Opt. Lett. **23** (June 1998), in press
8. M.K. Oshman, S.E. Harris: IEEE J. Quantum Electron. **QE-4**, 491 (1968)
9. T. Baer: J. Opt. Soc. Am. B**3**, 1175 (1986)
10. W. Jingyi, P. Mandel: Phys. Rev. A **48**, 671 (1993)
11. T. Debuisschert, J. Raffy, J.-P. Pocholle, M. Papuchon: J. Opt. Soc. Am. B**13**, 1569 (1996)
12. A. Ashkin, J.E. Bjorkholm: US Patent Application 808,767 (1969)
13. R.G. Smith, J.V. Parker: J. Appl. Phys. **41**, 3401 (1970)
14. E.O. Ammann, J.M. Yarborough, M.K. Oshman, P.C. Montgomery: Appl. Phys. Lett. **16**, 309 (1970)
15. J. Falk, J.M. Yarborough, E.O. Ammann: IEEE J. Quantum Electron. **QE-7**, 359 (1971)
16. V.I. Emel'yanov: Sov. J. Quantum Electron. **2**, 524 (1973)
17. Tran-Ba-Chu, M. Broyer: J. Physique **45**, 1599 (1984)
18. D.C. Edelstein, E.S. Wachman, C.L. Tang: Appl. Phys. Lett. **54**, 1728 (1989)
19. A. Kaz, L.R. Marshall: Conference on Lasers and Electro-Optics, Vol. 11 of 1993 OSA Technical Digest Series (Optical Society of America, Washington, DC 1993) p. 244–245
20. A.E. Siegman: Appl. Opt. **1**, 739 (1962)
21. W.R. Bosenberg, A. Drobshoff, J.I. Alexander, L.E. Myers, R.L. Byer: Opt. Lett. **21**, 713 (1996)
22. K. Schneider, P. Kramper, S. Schiller, J. Mlynek: Opt. Lett. **22**, 1293 (1997)
23. S.E. Harris: IEEE J. Quantum Electron. **QE-2**, 701 (1966)
24. J. La Salle, S. Lefschetz: *Stability by Liapunov's Direct Method with Applications* (Academic Press, London 1961)
25. W. Brunner, H. Paul: Ann. Phys. **7**, 180 (1972)
26. M. Scheidt, C. Becher, M.E. Klein, D.H. Lee, K.-J. Boller, R. Wallenstein: QELS 1997 paper QWG1